A Novel Robust Sensorless Technique for Field-Oriented Control Drive of Permanent Magnet Synchronous Motor

THAT-DONG TON[1]**, (Member, IEEE), MIN-FU HSIEH**[1]**, (Senior Member, IEEE), AND PO-HSUN CHEN**[2]**, (Member, IEEE)**
[1]Department of Electrical Engineering, National Cheng Kung University, Tainan 701, Taiwan
[2]Department of Applied Science, R.O.C. Naval Academy, Kaohsiung 81345, Taiwan

Corresponding author: Min-Fu Hsieh (mfhsieh@mail.ncku.edu.tw)

ABSTRACT This paper proposes a novel rotor position estimation technique based on stator flux linkage to implement robust sensorless field-oriented control for permanent magnet synchronous motor drives. The proposed method can accurately estimate rotor position by mitigating the dependence on quality of the magnitude and phase angle of the estimated stator flux linkage. A high-accuracy load angle calculation based on d-q-axis current estimation method is first developed for further rotor position determination. In the rotor position calculation, the reference flux linkage magnitude is used instead of the estimated one to avoid the influence of potential high noise levels during low speed operation. As a result, the rotor angle estimation depends only on the phase angle of stator flux linkage, without the effect of its magnitude. The estimation accuracy can thus be improved. Also, by employing a simple stator flux linkage phase lag compensator, the performance of the proposed sensorless method can be dramatically improved at low speed. Moreover, the problem of motor parameter variation (e.g., changes in winding resistance, stator inductances, and permanent magnetic flux linkage) has been analyzed and overcome. Finally, comparisons between conventional and proposed methods are presented with simulations and experiments to demonstrate the effectiveness and reliability of the proposed method.

INDEX TERMS Sensorless, field-oriented control, permanent magnet motor drive, sensorless vector control, current estimation, rotor position estimation, load angle estimation.

I. INTRODUCTION

In recent decades, the "greener" industrial policies have been extensively considered in the rising global demand for electrical and electronic products. As one such example, the permanent magnet synchronous motor (PMSM) is an outstanding candidate for variable-speed industrial drives due to its functional advantages, such as a wide constant power speed range, high efficiency, high power and torque density, and low maintenance [1]. To exploit the full PMSM potential, a high-performance drive plays a crucial role. So far, the field-oriented control (FOC) has been proven to be a typical technique for high-performance variable speed drives [1], which is suitable for most types of PMSMs. In the FOC scheme,

The associate editor coordinating the review of this manuscript and approving it for publication was Kan Liu.

the position information of the rotor is an indispensable requirement for both current and speed control loops. However, encoders are often bulky, costly, and sensitive to harsh industrial environments. Moreover, great care is required in their installations to achieve satisfactory accuracy. Therefore, some sensorless rotor position estimation algorithms have been developed to avoid these limitations [2]–[21].

Sensorless control (SLC) can be divided into three categories [2]–[4]. The first two are: 1) high frequency signal injection (HFI) technique [4], [10], [17] for tracking the magnetic saliency for low speeds or standstill operation, and 2) model-based observer technique for medium- to high-speed operations, where the information of the back electromotive force (B-EMF) [5]–[10], [21] or stator flux linkage [11]–[19] is observed from the measured phase voltage and current. Thus, if operations for a full speed range are

needed, a combined solution (i.e., the third category) of the above two categories is recommended [4], [10], [17].

In the model-based techniques (the second category), measured current errors or harmonics can occur when identifying motor parameters and rotor position in SLC FOC drives. Several methods have been developed to overcome this issue, such as model reference adaptive system (MRAS), sliding mode observer (SMO), and extended Kalman filter (EKF). For the MRAS, a modified algorithm to detect permanent magnet (PM) flux linkage and stator resistance achieves better stability at low speeds [6], but many unwieldy adjustors and filters are required. Similar conditions were found in the EKF, whose massive computation requires a strong processor. Nevertheless, the EKF is effective, robust to disturbance, and highly precise [7], [8]. The SMO has been widely studied for SLC FOC drives over the last decades because it is relatively easy to construct. Its effectiveness is independent of external disturbances and mismatch parameters [5]. However, the chattering characteristic significantly affects the accuracy and quality of controllers. A phase-locked-loop (PLL) technique and filter are often used to suppress the noise resulting from the speed signals extracted, again adding some complexity. Recently, an adaptive SMO method has been proposed [21] to reduce chattering, but the design of many observer parameters has not been described in detail.

The SLC method based on stator flux linkage vector is classified in the model-based (second) category. Unlike the methods mentioned above, the flux-linkage-based SLC method is often investigated associated with a direct torque control (DTC) or stator-FOC drive scheme. In this case, the rotor angle can be extracted from the rotor or stator flux linkage vector. Therefore, if the stator/rotor flux linkage information is known, the motor operation state can be identified. It is well-known that the "active flux" method is an extended rotor flux linkage model commonly used [12], [13]. It enables a simple drive scheme over a wide speed range, even at low speed, with an adapted stator flux linkage observer structure [12], [15], [18]. The rotor angle can also be provided indirectly from the stator flux vector using other methods [11], [19], e.g., through a calculation based on load angle and stator flux linkage angle. Overall, the common difficulty for the flux-linkage-based SLC is that the rotor position estimation relies heavily on the accuracy of the estimated stator flux linkage magnitude and angle, which can be easily influenced by factors such as variation of resistance and potential nonlinearity with low B-EMF at high current. Hence, recent studies mostly focus on enhancing the accuracy of the stator flux linkage estimator [14], [15], [18], [26] rather than developing methods to reduce the dependence on stator flux linkage components (i.e., magnitude and phase angle) in SLC calculations.

From the above discussion, the main objective of this study is to avoid a direct and strong connection between rotor position estimation and stator flux linkage components. Therefore, a novel SLC calculation approach is proposed in this paper to improve the performance of the PMSM SLC FOC
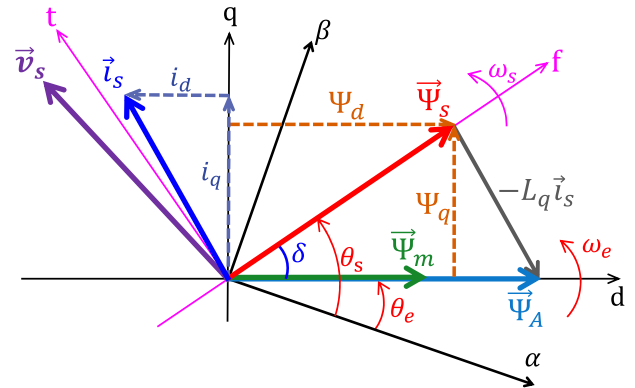

FIGURE 1. Phasor diagram used in analysis of PMSM drive.

drive by reducing the dependence on the stator flux linkage components when estimating the rotor position. The proposed method is sufficiently robust for the PMSM to operate at low speed (e.g., 100 rpm) without complex regulators. The main features of this study are:

1) A new method is developed to estimate the *d-q*-axis currents based on the mathematical model of PMSMs for load angle calculation. This is to reduce the influence of the stator flux linkage phase angle estimation on load angle calculation for further rotor position acquisition. This technique has not been reported elsewhere.

2) The rotor position accuracy can be further improved by reducing the potential influence of imprecision of the stator flux linkage estimation. This is achieved by replacing the magnitude of the estimated stator flux linkage with that of the reference one. Moreover, the phase lag of the estimated stator flux linkage phase angle at low speed is compensated to enhance the rotor position accuracy.

3) The robustness of the proposed SLC is investigated. This includes a sensitivity analysis for motor parameter variation on the rotor angle estimation. A method is developed to mitigate the effects of motor parameter mismatch. A novel detection method is also developed for the variation of the PM flux linkage at high speed.

Simulations and experiments are conducted to validate the proposed method.

II. PMSM MATHEMATICAL MODEL

For convenience, the nomenclatures used in this paper are defined in Table 1.

The stator voltage vector in PMSM can be expressed as:

$$\vec{v}_s = R_s \vec{i}_s + \frac{d\vec{\Psi}_s}{dt} \qquad (1)$$

The relationships between stator/rotor flux linkage, voltage, and current of PMSM under different coordinates are represented in the phasor diagram, as shown in Fig. 1.

According to Fig. 1, the voltage equation in the *d-q* frame can be written as:

$$\begin{bmatrix} v_d \\ v_q \end{bmatrix} = R_s \begin{bmatrix} i_d \\ i_q \end{bmatrix} + \frac{d}{dt} \begin{bmatrix} \Psi_d \\ \Psi_q \end{bmatrix} + \omega_e \begin{bmatrix} -\Psi_q \\ \Psi_d \end{bmatrix} \qquad (2)$$

TABLE 1. Nomenclature.

Symbol	Definition
$\vec{v}_s$, $\vec{i}_s$, and $\vec{\Psi}_s$	Stator voltage, current, and flux linkage vector.
$\begin{bmatrix} v_d \\ v_q \end{bmatrix}$, $\begin{bmatrix} i_d \\ i_q \end{bmatrix}$, and $\begin{bmatrix} \Psi_d \\ \Psi_q \end{bmatrix}$	Element matrices of stator voltages, stator currents, and stator flux linkages in d-q-axis on rotor rotating coordinate.
$\begin{bmatrix} v_\alpha \\ v_\beta \end{bmatrix}$, $\begin{bmatrix} i_\alpha \\ i_\beta \end{bmatrix}$, and $\begin{bmatrix} \Psi_\alpha \\ \Psi_\beta \end{bmatrix}$	Element matrices of stator voltages, stator currents, and stator flux linkages in α-β-axis on stationary coordinate.
$\Psi_s = \sqrt{\Psi_\alpha^2 + \Psi_\beta^2}$	Magnitude of stator flux linkage.
i_{abc}	Three phase currents.
$i_s = \sqrt{i_\alpha^2 + i_\beta^2}$	Magnitude of stator current.
i_f and i_t	Stator currents in f-t-axis on stator flux linkage rotating coordinate.
R_s	Stator resistance.
Ψ_m	Magnitude of permanent magnet flux linkage.
L_d and L_q	Stator inductances in the d-q-axis.
Ψ_A and θ_A	Magnitude and phase angle of active flux vector
$\Psi_{A\alpha}$ and $\Psi_{A\beta}$	Element rotor flux linkages in α-β-axis.
θ_s	Stator flux linkage angle.
θ_e	Electrical angle named as "rotor angle".
δ	Load angle.
ω_s	Stator flux linkage speed.
ω_e	Electrical angular speed.
ω_m	Mechanical angular speed of rotor.
p_p	Pole-pair number of PMSM.
T_e	Electromagnetic torque.
*	Reference/command quantities.
^	Estimated/observed quantities.
Δ	Deviation quantities.
~	Updated quantities.

where the stator flux linkages of the PMSM in the d-q frame can be expressed by:

$$\begin{bmatrix} \Psi_d \\ \Psi_q \end{bmatrix} = \begin{bmatrix} L_d \\ & L_q \end{bmatrix} \begin{bmatrix} i_d \\ i_q \end{bmatrix} + \begin{bmatrix} \Psi_m \\ 0 \end{bmatrix} \tag{3}$$

$$\Psi_s = \sqrt{\Psi_d^2 + \Psi_q^2} \tag{4}$$

As shown in Fig. 1, the d-q-axis stator flux linkage can also be described based on the relationship between the load angle and stator flux linkage as:

$$\begin{bmatrix} \Psi_d \\ \Psi_q \end{bmatrix} = \Psi_s \begin{bmatrix} \cos\delta \\ \sin\delta \end{bmatrix} \tag{5}$$

$$\delta = \tan^{-1}\left(\frac{\Psi_q}{\Psi_d}\right) \tag{6}$$

The electromagnetic torque equations of the PMSM in d-q and $\alpha - \beta$ frames are respectively given as:

$$T_e = \frac{3}{2} p_p \left[\Psi_m + (L_d - L_q) i_d \right] i_q \tag{7a}$$

and

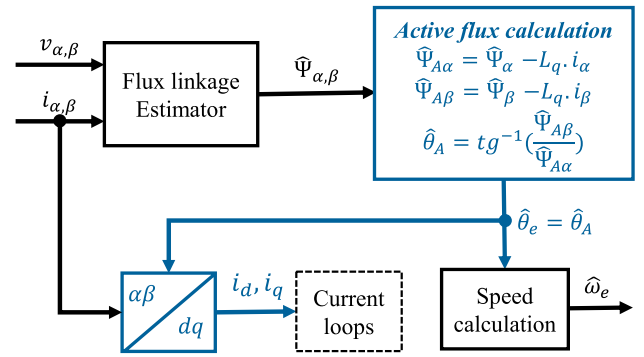$$T_e = \frac{3}{2} p_p (\Psi_\alpha i_\beta - \Psi_\beta i_\alpha) \tag{7b}$$

FIGURE 2. Conventional SLC scheme based on "active flux" vector, reproduced from [12].

The current magnitude is calculated by:

$$i_s = \sqrt{i_d^2 + i_q^2} \tag{8}$$

Also, as shown Fig. 1, the active flux vector [13] can be expressed as:

$$\vec{\Psi}_A = \vec{\Psi}_s - L_q \vec{i}_s \tag{9}$$

where

$$\Psi_A = \Psi_m + (L_d - L_q) i_d \tag{10}$$

The active flux vector will be further used in the following derivation.

III. BRIEF REVIEW OF CONVENTIONAL SENSORLESS CONTROL METHODS BASED ON FLUX LINKAGE

In the SLC FOC scheme, the rotor angle information plays a crucial role, which allows the rotor speed to be derived, and the Park/Clark transformations to be performed. Therefore, the high accuracy of rotor angle estimation is key to the robustness of the SLC-FOC scheme. In conventional SLC methods based on flux linkage, the rotor angle can be estimated in two ways: 1) directly based on the active flux vector ($\vec{\Psi}_A$ shown in Fig. 1, denoted "active flux SLC") [12], [13], [17], and 2) indirectly via the load angle (δ) calculated by f-t-axis currents and stator flux linkage angle [19] (denoted "f-t-axis current SLC"). For the former method, the determination of rotor angle and d-q-axis currents of the conventional SLC technique [12] is shown in Fig. 2. From (9), the calculation of active flux vectors in the stationary coordinate is expressed as

$$\begin{bmatrix} \Psi_{A\alpha} \\ \Psi_{A\beta} \end{bmatrix} = \begin{bmatrix} \Psi_\alpha \\ \Psi_\beta \end{bmatrix} - L_q \begin{bmatrix} i_\alpha \\ i_\beta \end{bmatrix} \tag{11}$$

$$\theta_e = \theta_A = \tan^{-1}\left(\frac{\Psi_{A\beta}}{\Psi_{A\alpha}}\right) \tag{12}$$

It can be realized from (11), (12), and Fig. 2 that the calculation process of rotor angle in the active flux SLC method is quite simple with only a few computation steps. However, the accuracy of this angle strongly depends on the quality of both amplitude and phase angle of the estimated stator flux linkage vector and measured current vector.

In the latter technique (indirect calculation method), as can be seen in Fig. 1, the stator flux linkage vector $\vec{\Psi}_s$ deviates with the d-axis in the rotor coordinate by the load angle δ. Thus, once the load angle and stator flux linkage angle are determined, the rotor angle can be obtained by:

$$\theta_e = \theta_s - \delta \tag{13}$$

where the stator flux linkage angle θ_s can be easily calculated from the α-β-axis stator flux linkage, as given by:

$$\theta_s = \tan^{-1}\left(\frac{\Psi_\beta}{\Psi_\alpha}\right) \tag{14}$$

In [19], the load angle is computed by the stator flux linkage magnitude and f-t-axis currents with the equation expressed below:

$$\delta = \tan^{-1}\left(\frac{L_q i_t}{\Psi_s - L_q i_f}\right) \tag{15}$$

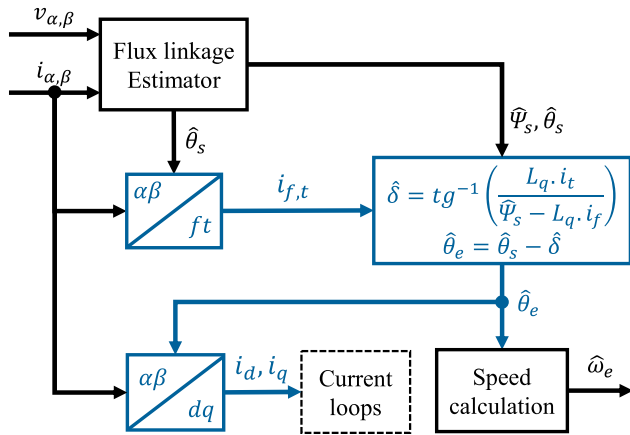This SLC scheme [19] is reproduced as in Fig. 3.

FIGURE 3. Conventional SLC scheme based on indirect calculation from stator flux linkage and *f-t*-axis currents, reproduced from [19].

From the rotor angle calculation process shown in Fig. 3, the result depends on the magnitude and phase angle of the stator flux linkage vector, where the phase angle is twice involved. Hence, the accuracy of rotor angle estimation is dramatically sensitive to the estimated stator flux linkage angle. Furthermore, the equivalent mathematical transformations between the active flux method and the *f-t*-axis current method [19] have the same degree of dependence on the stator flux linkage vector. Therefore, reducing this dependence is necessary to improve the performance of SLC-FOC drives based on stator flux linkage.

To summarize the above discussion, the load/rotor angles should be deduced by other means to avoid their strong connection with phase angle and magnitude of the estimated stator flux linkage. Thus, in this work, the load angle is instead deduced from the estimated *d-q*-axis current (to be detailed in Section IV), and the sensitivity to the inaccuracies of the estimated stator flux linkage magnitude and phase angle can be reduced compared to the previously mentioned methods. Consequently, this would improve the accuracy of rotor position estimation.

IV. PROPOSED ROTOR ANGLE ESTIMATION BASED ON D-Q-AXIS CURRENT ESTIMATION

In this section, a method for estimating *d-q*-axis currents is presented. Note that the feedback *d-q*-axis currents obtained by Clarke/Park transformations are still used for the current control loop in the complete SLC-FOC scheme. The estimated *d-q*-axis currents are mainly used here for the rotor/load angle calculation to improve accuracy.

A. PROPOSED ESTIMATION OF DQ-AXIS CURRENTS

The *d-q*-axis current can be obtained from the fundamental equations of stator flux linkage expressed in the *d-q* frame. Substituting (3) into (4) gives:

$$\Psi_s^2 = (\Psi_m + L_d i_d)^2 + (L_q i_q)^2 \tag{16}$$

The quadrature current is re-written from (8) to be:

$$i_q^2 = i_s^2 - i_d^2 \tag{17}$$

Substituting (17) into (16), a quadratic equation of *d*-axis current is found to be:

$$(L_q^2 - L_d^2)i_d^2 - 2\Psi_m L_d i_d + (\Psi_s^2 - \Psi_m^2 - L_q^2 i_s^2) = 0 \tag{18}$$

If $L_d \neq L_q$, then Equation (18) is solved according to i_d. The two solutions i_{d1} and i_{d2} are acquired as below:

$$i_{d1} = \frac{\Psi_m L_d}{(L_q^2 - L_d^2)} \\ - \frac{\sqrt{(L_q^2 - L_d^2)L_q^2 i_s^2 - (L_q^2 - L_d^2)\Psi_s^2 + L_q^2 \Psi_m^2}}{(L_q^2 - L_d^2)} \tag{19}$$

$$i_{d2} = \frac{\Psi_m L_d}{(L_q^2 - L_d^2)} \\ + \frac{\sqrt{(L_q^2 - L_d^2)L_q^2 i_s^2 - (L_q^2 - L_d^2)\Psi_s^2 + L_q^2 \Psi_m^2}}{(L_q^2 - L_d^2)} \tag{20}$$

with the following condition to satisfy:

$$(L_q^2 - L_d^2)L_q^2 i_s^2 - (L_q^2 - L_d^2)\Psi_s^2 + L_q^2 \Psi_m^2 \geq 0 \tag{21}$$

In the case of an interior permanent magnet synchronous motor (IPMSM), to examine the operating capability to satisfy the condition in (21), a mathematical analysis is conducted. For a common IPMSM, there are two characteristics: 1) $L_d < L_q$, thus the two solutions to (18) are $i_{d1} \leq 0$ and $i_{d2} \geq 0$; 2) $i_d \leq 0$. Therefore, the negative i_{d1} is chosen for calculation and evaluation.

The stator flux linkage in (21) is converted into a new inequality as:

$$\Psi_s^2 \leq \frac{L_q^2 \Psi_m^2}{(L_q^2 - L_d^2)} + L_q^2 i_s^2 \tag{22}$$

From (22), the limit value of Ψ_s can be deduced to be:

$$\Psi_s^{\lim} = \sqrt{\frac{L_q^2 \Psi_m^2}{(L_q^2 - L_d^2)} + L_q^2 i_s^2} \tag{23}$$

TABLE 2. Specifications for the target IPMSM.

Specification	Value	Unit (SI)
DC voltage V_{dc}	150	V_{DC}
Rated current i_{rated}	15	A_{pk}
Maximum current i_{max}	25	A_{pk}
Base speed N_{base}	2000	rpm
Rated torque $T_{e,rated}$	5.0	N.m
Pole-pairs p_p	4	-
Stator resistance R_s	175	$m\Omega$
Permanent magnet flux linkage Ψ_m	86.5	mWb
d-axis inductance L_d	0.76	mH
q-axis inductance L_q	1.63	mH

where $\Psi_s^{\lim}$ is the stator flux linkage limit. If the actual stator flux linkage Ψ_s at every operating point is lower than $\Psi_s^{\lim}$, the solution for i_{d1} is available for all states. As known, under low speed operation of IPMSM, the actual stator flux linkage is often controlled to reach the expected value, which is determined either by maximum torque per ampere (MTPA) or at $i_d = 0$. The stator flux linkages in these two conditions are denoted Ψ_s^{mtpa} and $\Psi_s^{i_d=0}$, respectively. It is apparent that the stator flux linkage in the $i_d = 0$ case is greater than that in the MTPA one ($\Psi_s^{i_d=0} > \Psi_s^{mtpa}$) because the field could be slightly weakened during the MTPA operation [21]. Therefore, $\Psi_s^{i_d=0}$ is chosen to compare with the stator flux linkage limit $\Psi_s^{\lim}$ above. The calculation equation of $\Psi_s^{i_d=0}$ is:

$$\Psi_s^{i_d=0} = \sqrt{\Psi_m^2 + L_q^2 i_s^2} \tag{24}$$

Assuming that $\Psi_s^{i_d=0} \leq \Psi_s^{\lim}$, the following equation can be obtained:

$$\sqrt{\Psi_m^2 + L_q^2 i_s^2} \leq \sqrt{\frac{L_q^2 \Psi_m^2}{(L_q^2 - L_d^2)} + L_q^2 i_s^2} \tag{25}$$

Simplifying (25) yields:

$$\sqrt{\frac{L_q^2}{(L_q^2 - L_d^2)}} \geq 1 \tag{26}$$

Since $L_d < L_q$ for IPMSM, inequality (26) is valid for all the considered operating states. It can be concluded that the condition in (21) is constantly satisfied for IPMSM, meaning that the solution i_{d1} constantly exists. To clarify this, the simulation result in Fig. 4 compares the stator flux linkages curves of $\Psi_s^{\lim}$, Ψ_s^{mtpa}, and $\Psi_s^{i_d=0}$ of the IPMSM with the specifications given in Table 2. As can be seen, the curve of $\Psi_s^{\lim}$ is constantly higher than that of $\Psi_s^{i_d=0}$ and Ψ_s^{mtpa} over the entire operating range. This result supports the above statement.

Thus, the equation used for calculating d-axis current of IPMSM is (19). It can thus be re-written as:

$$\hat{i}_d^{ipm} = A - \sqrt{B.i_s^2 - C.\hat{\Psi}_s^2 + D} \tag{27}$$

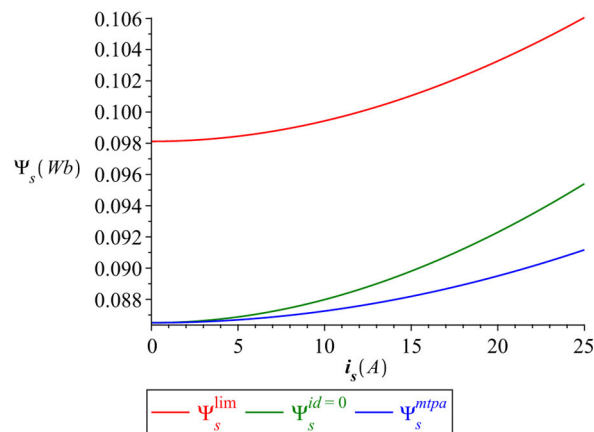**FIGURE 4.** Comparison of $\Psi_s^{\lim}$, Ψ_s^{mtpa}, and $\Psi_s^{i_d=0}$ curves of IPMSM.

where $\hat{i}_d^{ipm}$ is the estimated d-axis current for IPMSM. The constants A, B, C, and D are assigned as below:

$$A = \frac{\Psi_m L_d}{(L_q^2 - L_d^2)} \quad B = \frac{L_q^2}{(L_q^2 - L_d^2)}$$

$$C = \frac{1}{(L_q^2 - L_d^2)} \quad D = \frac{L_q^2 \Psi_m^2}{(L_q^2 - L_d^2)}$$

On the other hand, in the case of a surface permanent magnet synchronous motor (SPMSM), $L_d = L_q = L_s$, where L_s is stator inductance. Thus, (18) can be simplified as:

$$-2\Psi_m L_s i_d + (\Psi_s^2 - \Psi_m^2 - L_s^2 i_s^2) = 0 \tag{28}$$

Equation (28) has only one solution for d-axis current $\hat{i}_d^{spm}$ as:

$$\hat{i}_d^{spm} = \frac{\hat{\Psi}_s^2 - \Psi_m^2 - L_s^2 i_s^2}{2\Psi_m L_s} \tag{29}$$

Since $\Psi_m \neq 0$ and $L_s \neq 0$ for SPMSM, the solution $\hat{i}_d^{spm}$ in (29) is constantly valid.

The q-axis current $\hat{i}_q$ is deduced from torque equation (7a) and is given as:

$$\hat{i}_q = \frac{\hat{T}_e}{3/2 p_p (\Psi_m + (L_d - L_q)\hat{i}_d)} \tag{30}$$

These estimation values $\hat{i}_d$ and $\hat{i}_q$ are used to calculate load angle $\hat{\delta}$ and rotor angle $\hat{\theta}_e$ in the next stage.

B. ESTIMATION OF STATOR FLUX LINKAGE AND ELECTROMAGNETIC TORQUE

For simplicity, the stator flux linkage estimation technique used here is a typical closed-loop estimator based on low-pass filter (LPF) with the adaptive compensation [20], [26], as re-constructed in Fig. 5. Via the diagram in Fig. 5, the magnitude ($\hat{\Psi}_s$) and phase angle ($\hat{\theta}_s$) of stator flux linkage and the electromagnetic torque ($\hat{T}_e$) can be determined.
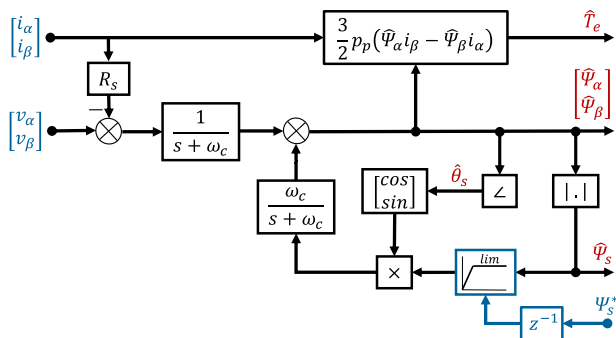
FIGURE 5. Stator flux linkage and electromagnetic torque estimation, redrawn from [20], where ω_c is the cutoff-frequency of LPF estimator.

C. PROPOSED ROTOR ANGLE ESTIMATION-METHOD 1

The rotor angle $\hat{\theta}_e$ is extracted from the estimated stator flux linkage phase angle $\hat{\theta}_s$ and load angle $\hat{\delta}$ as given in (13), where $\hat{\delta}$ can be calculated by (6), as re-written to be:

$$\hat{\delta} = \tan^{-1}\left(\frac{L_q\hat{i}_q}{\Psi_m + L_d\hat{i}_d}\right) \quad (31)$$

where $\hat{i}_d$ is estimated by (27) for IPMSM or (29) for SPMSM, and $\hat{i}_q$ is calculated by (30).

The first proposed SLC calculation process (Method 1, denoted PP-01) for PMSM is presented in the block diagram shown in Fig. 6.

The implementation steps in Fig. 6 are explained as follows:

Step 1 (S1): The measured 3-phase currents and the 3-phase voltages deduced by switching states are converted into $i_{\alpha,\beta}$ and $v_{\alpha,\beta}$, respectively via Clarke transformation. Then, the $\hat{\Psi}_s$, $\hat{\theta}_s$, and $\hat{T}_e$ are estimated using diagram shown in Fig. 5. Also, the current magnitude i_s is obtained by $i_{\alpha,\beta}$.

Step 2 (S2): The estimated d-axis current $\hat{i}_d$ is calculated based on i_s and $\hat{\Psi}_s$ obtained in S1 by (27) for IPMSM, or (29) for SPMSM.

Step 3 (S3): The estimated q-axis current $\hat{i}_q$ is determined by (30) from $\hat{i}_d$ in S2 and $\hat{T}_e$ in S1.

Step 4 (S4): The load angle $\hat{\delta}$ is calculated by (31) with the acquired $\hat{i}_d$ and $\hat{i}_q$ in S2 and S3, respectively.

Step 5 (S5): The rotor angle $\hat{\theta}_e$ is obtained by subtracting $\hat{\delta}$ in S4 from $\hat{\theta}_s$ in S1.

Step 6 (S6): The rotor angular speed $\hat{\omega}_e$ is extracted from the derivative of $\hat{\theta}_e$ in S5 over time as:

$$\hat{\omega}_e = \frac{d\hat{\theta}_e}{dt} \quad (32)$$

An LPF is used to reduce the high-frequency noise of the speed output signals (note that this LPF for the speed calculation is different from that for stator flux linkage estimator as mentioned previously). As mentioned before, the d-q-axis currents ($i_{d,q}$) feedback to current control loops are collected from Park transformation of $i_{\alpha,\beta}$ with $\hat{\theta}_e$.

According to the calculation procedures mentioned above, it is apparent that the load angle calculation in PP-01 is independent of the stator flux linkage phase angle, whose
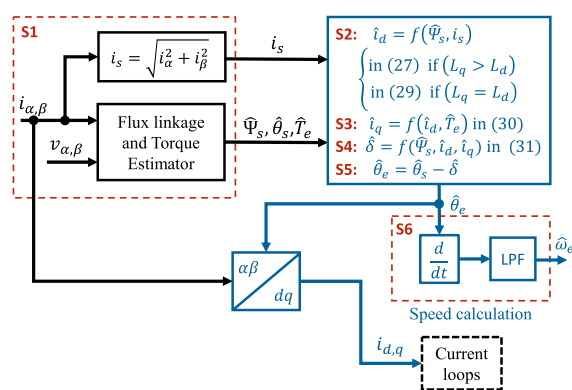

FIGURE 6. The proposed sensorless scheme (PP-01) for PMSM.

impact on the accuracy of the rotor angle estimation is thus reduced dramatically compared to conventional methods. The effectiveness of PP-01 on the IPMSM SLC-FOC drive system is evaluated and discussed below.

D. COMPARISON OF METHOD PP-01 AND CONVEN-TIONAL SLC METHOD

To examine the improvement of the first proposed method (PP-01) compared to conventional ones, the accuracy of the feedback d-q-axis currents, load angle, and rotor angle is compared via simulation.

As a benchmark, a standard FOC drive system with a rotor position sensor is used to drive the target IPMSM (Table 2). The SLC calculations using the proposed method and a conventional method are respectively implemented on the benchmarking FOC system. The conventional SLC method is the scheme based on f-t-axis current as shown in the diagram in Fig. 3 (named CONV). The proposed SLC method (PP-01) was previously explained, as shown in Fig. 6. The deviations in terms of rotor/load angles and currents between the benchmark FOC drive and the two SLC schemes using MATLAB simulation are presented, as shown in Fig. 7.

The considered operation conditions are given in Fig. 7(a), where the stator resistance is assumed to increase to 130% due to temperature. Thus, the stator flux linkage estimation could be significantly affected at low speed (i.e., the magnitude attenuation and phase lag) with the LPF flux linkage estimator presented in refs. [18], [26].

From the results shown in Figs. 7(b) and 7(c), the rotor/load angle results for PP-01 (red curve) have smaller errors than those of CONV (blue curve) under the circumstance of possible low accuracy of stator flux linkage estimation at speeds below 700 rpm. The d-q-axis feedback current of PP-01 also has less deviation, as shown in Figs. 7(d) and 7(e). This result demonstrates that the proposed SLC method is more effective than the conventional one.

The above result reveals that in the proposed method (PP-01), the reduced involvement of the estimated stator flux linkage in load/rotor angle calculation is proved to be effective.

However, the errors of the d-q-axis current and rotor angle estimation in the proposed PP-01 method are still large at
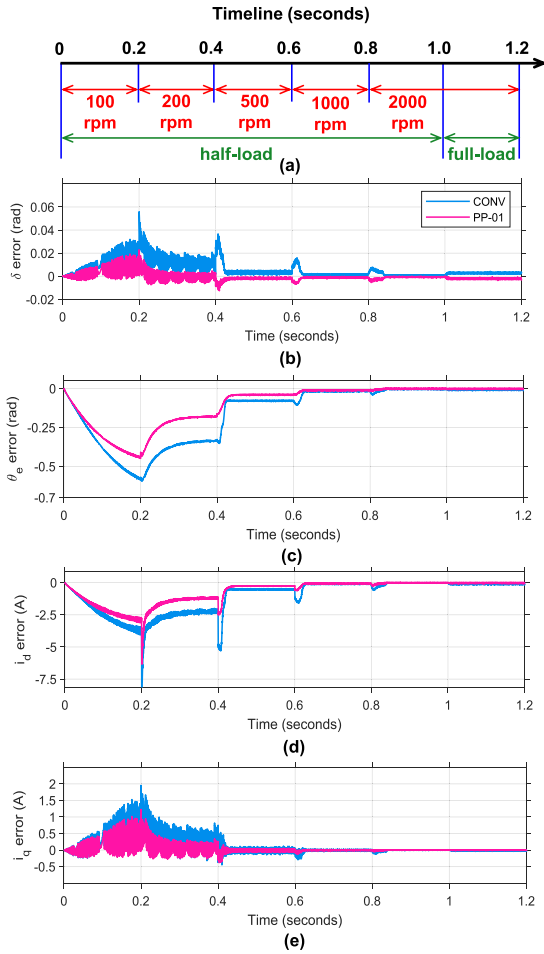
FIGURE 7. Simulation comparison between CONV and PP-01 SLC methods: (a) the operating conditions with stator resistance increasing to 130%, (b) load angle error, (c) rotor angle error, (d) *d*-axis feedback current error, and (e) *q*-axis feedback current error.

speed below 200 rpm. This may be due to the phase lag of the stator flux linkage estimation caused by the LPF estimator [18], [25] and the possible nonlinearity of the inverter and PMSM [26]. This may cause the closed-loop SLC-FOC drive system to be unstable at low speeds. Hence, the quality of the estimation should be further improved.

E. IMPROVEMENT FOR PROPOSED ROTOR ANGLE ESTIMATION-METHOD 2

According to (27), (29), (30), and (31), it can be realized that the incorrect magnitude estimated of stator flux linkage influences the estimation result of *d-q*-axis current and load angle. To avoid this, the value $\hat{\Psi}_s$ in (27) and (29) can be replaced by reference stator flux linkage in the previous step. The reference stator flux linkage magnitude Ψ_s^* is calculated by the reference *d-q*-axis currents $i_{d,q}^*$ as:

$$\Psi_s^* = \sqrt{(\Psi_m + L_d i_d^*)^2 + (L_q i_q^*)^2} \qquad (33)$$

In the low-speed zone, the phase lag condition of stator flux linkage can be severe due to the previously mentioned LPF estimator and the nonlinearity of the inverter and PMSM.
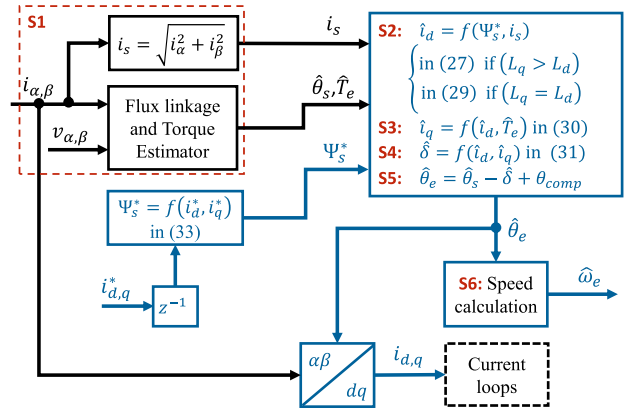
FIGURE 8. The second proposed sensorless scheme (PP-02) for PMSM.

To solve the issue, a phase compensator is added to the output angle in the stator flux linkage estimation. If the rotor speed is lower than the cutoff frequency ($\omega_e < \omega_c$), the compensation angle θ_{comp} is expressed as [25], [26]

$$\theta_{comp} = -\tan^{-1}\left(\frac{\omega_c}{\omega_e}\right) \qquad (34)$$

Then, the rotor angle equation is updated to be

$$\hat{\theta}_e = \hat{\theta}_s - \hat{\delta} + \theta_{comp} \qquad (35)$$

Finally, the proposed sensorless scheme has been improved and re-constructed as the block diagram shown in Fig. 8 (denoted PP-02).

F. ANALYSIS AND DETECTION FOR VARIATION OF STATOR INDUCTANCE AND PM FLUX LINKAGE

The SLC scheme PP-02 shown in Fig. 8 involves many motor parameters, such as PM flux linkage and *d-q*-axis inductances. These parameters are often sensitive to varying operating conditions, such as large current (causing saturation) or high temperature (increasing winding resistance). In low-speed operation (below base speed), the PM flux linkage can be assumed to be stable without field weakening applied. Then, the effect of varying stator inductances on the load angle estimation for the CONV and PP-02 methods is examined and compared using simulation at rated current for the IPMSM given in Table 2. The schemes used in load angle calculation are shown in Fig. 3 and Fig. 8 for CONV and PP-02, respectively, and the simulation results are presented in Fig. 9. As can be seen, the L_d variation only has a slight effect on the estimated load angle of PP-02 in the case with increasing L_q and decreasing L_d simultaneously. Note that L_d does not affect the load angle of CONV according to (15) and Fig. 3. On the contrary, both CONV and PP-02 are substantially sensitive to L_q variation. Therefore, the influence of L_d can be neglected while the L_q variation should be determined and updated in the SLC during operation. To compensate the L_q variation for varying loads, the simple solution reported in [12] is applied. The inductance L_q variation as a function

of operating torque can be expressed as [12]

$$\tilde{L}_q = \frac{L_q}{(1 + K_t \frac{\hat{T}_e}{T_{e,rated}})} \qquad (36)$$

where $\tilde{L}_q$ is updated q-axis inductance according to the estimated torque $\hat{T}_e$, and K_t is the torque constant. Note that $\hat{T}_e$ is calculated by (7b); therefore, it is not affected by d-q-axis inductances and PM flux linkage. This then ensures the accuracy of the calculated L_q variation and load angle.

It should be noted that the estimation method of flux linkage angle shown in Fig. 5 is independent of d-q-axis inductances. However, the inductances are involved in load angle calculation, as can be seen in Fig. 8 (proposed method) and Fig. 3 (conventional method). In Fig. 9, the per-unit load angle plotted against d-q-axis inductances based on rated current allows the load angle error to be determined with inductance variation. This can then be used to further calculate the rotor angle error.

The PM flux linkage may vary with the degree of field weakening and temperature at high speeds. Since the stator flux linkage estimation is accurate at high speeds, the estimated load angle in (15) is nearly equal to (31). Therefore, to track the variation of PM flux linkage, the following equation is developed through (15) and (31):

$$\Delta\Psi_m = (\hat{\Psi}_s - \tilde{L}_q i_f)\frac{i_q}{i_t} - (\Psi_m + L_d i_d) \qquad (37)$$

$$\tilde{\Psi}_m = \Psi_m + \Delta\Psi_m \qquad (38)$$

where $\Delta\Psi_m$ is an amount of change of PM flux linkage and $\tilde{\Psi}_m$ is an updated value of PM flux linkage. Note that the q-axis inductance in (37) is updated from (36).

After the variation of motor parameters is detected and estimated, they are updated in the SLC calculation process.

V. BLOCK DIAGRAM OF COMPLETE PROPOSED SLC-FOC FOR IPMSM DRIVE

The block diagram of the complete SLC-FOC drive scheme for the IPMSM based on PP-02 is presented in Fig. 10. In this drive system, the speed and d-q-axis current control loops [23], as well as the maximum-torque-per-ampere (MTPA) algorithm, are designed using the methods presented in previous studies [24]. As previously mentioned, the stator flux linkage and torque estimator shown in Fig. 5 is adopted. The space vector pulse width modulation (SVPWM) is used to generate PWM pulses with a switching cycle T_s. For the hardware in the system, a voltage source inverter (VSI), 3-phase current sensors, a dc power supply, and the IPMSM (Table 2) are employed.

The calculation of motor parameter variation through (36) and (38) is performed online with a lower calculation (or update) frequency than that of the speed control loop (only one-tenth). This indicates that the period to update the q-axis inductance and PM flux linkage is ten times that of the speed control loop since the motor parameters do not change rapidly. As a result, the computation effort can be
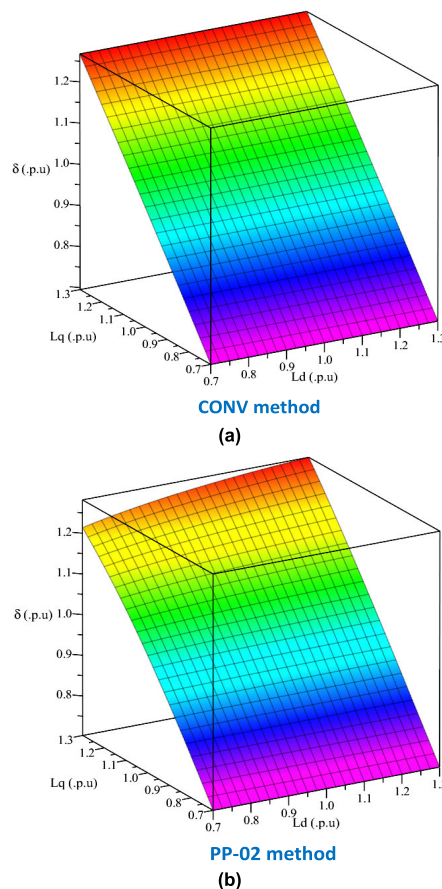

CONV method

(a)

PP-02 method

(b)

FIGURE 9. Comparison of effect of L_d and L_q variation on load angle estimation between (a) CONV and (b) PP-02 methods. (p.u. = 1.0 indicating load angle at rated condition).

greatly reduced. To start up the motor under light load, the current-frequency (I-F) technique [22] is employed. However, to avoid complexity, they are not exhibited in the block diagram shown in Fig. 10.

For the SLC calculation process, it seems that the proposed method with the additional online function of parameter variation detection might require more computation effort than conventional methods. However, for high-performance drives involving MTPA and field weakening control, this function is useful. Furthermore, from a schematic comparison between the PP-01, PP-02, and CONV methods, as shown in Fig. 11, PP-02 should be the most suitable and reliable solution to be applied.

VI. RESULTS

A. EXPERIMENT SETUPS

The proposed SLC FOC schemes were evaluated by the experiment results gathered from two test platforms: 1) the Hardware-In-the-Loop (HIL) toolkit shown in Fig. 12, and 2) a testbench shown in Fig. 13, for the IPMSM given in Table 2. With the HIL device serving as a real-time test platform for the motor drive system [27], [28], the correctness and performance of the proposed SLC-FOC control algorithms written in a micro control unit (MCU) (TMS320F28379D,
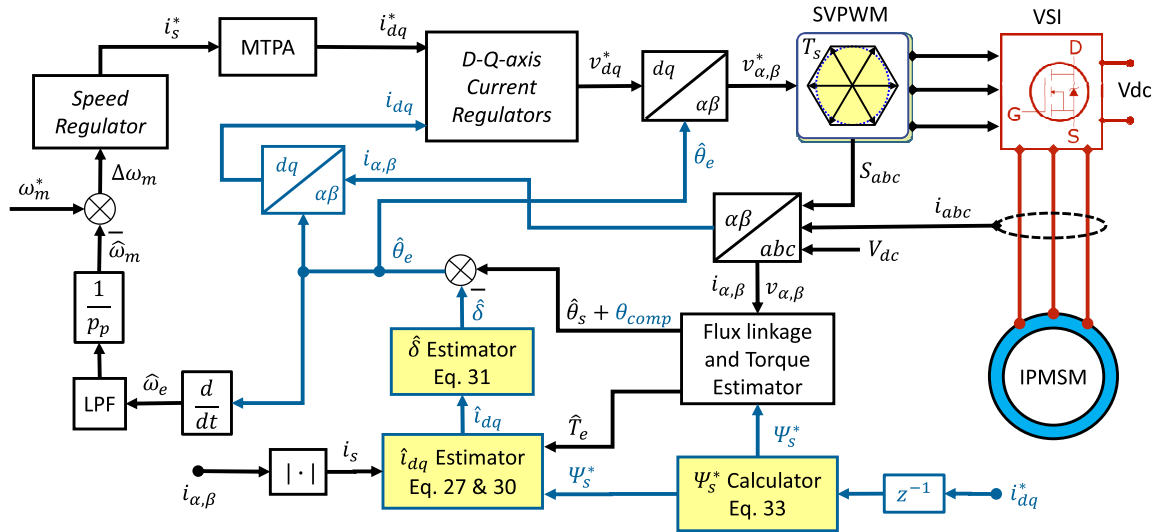
FIGURE 10. Block diagram of the complete proposed SLC-FOC scheme for IPMSM drive.
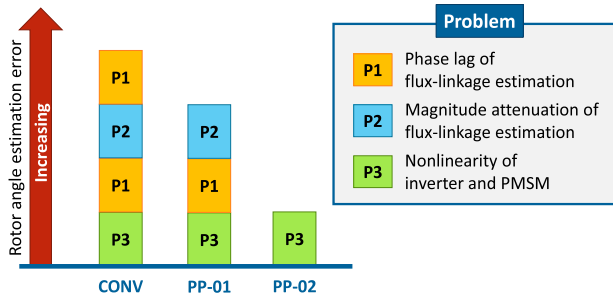

FIGURE 11. The comparison of improvement between the rotor angle estimation methods: CONV, PP-01, and PP-02.

also called DSP here) can be tested and preliminarily evaluated. The mathematical model of the IPMSM with the specifications listed in Table 2 is built in the HIL. The switching frequency of the VSI in the HIL and testbench is 10 kHz. The rotor position and three-phase current signals from the sensors are fed back to the MCU as a reference for comparison.

The gains of all the regulators are designed to be: $K_{p,\omega} = 1.539$ and $K_{i,\omega} = 0.138$ for the Proportional and Integral (PI) controller of the speed loop; $K_{p,id} = 4.775$ and $K_{i,id} = 1099.6$ for that of the d-axis current loop; $K_{p,iq} = 10.116$ and $K_{i,iq} = 1099.6$ for that of the q-axis current loop. The command update rates are 5 kHz and 1 kHz for current and speed loops, respectively.

The I-F technique [22] is applied under light load (1 Nm) as previously mentioned to start up the motor.

B. COMPARISON OF PROPOSED AND CONVENTIONAL SLC METHODS

To verify the performance of the proposed methods (PP-01 and PP-02 shown in Figs. 6 and 8, respectively) and compare with conventional SLC methods (that are based on the "*f-t*-axis current" model in Fig. 3), the tests are conducted in the HIL platform by step-braking the motor under a slight load (1 Nm) gradually from 2000 rpm to 100 rpm. This aims
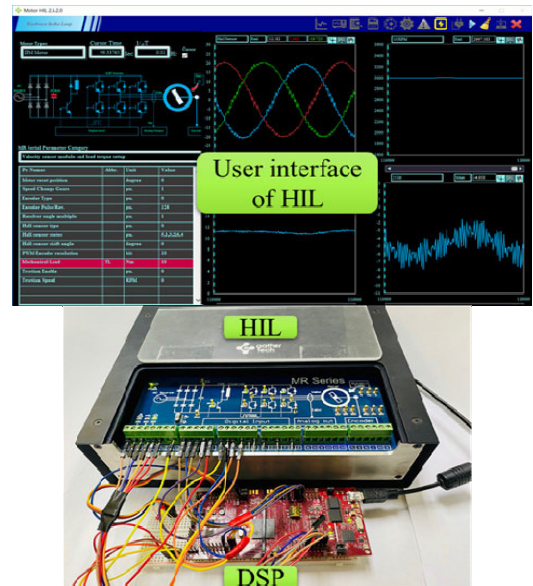

FIGURE 12. Experimental platform with HIL MR series II.

to test the lowest achievable speed of each method (shown in Figs. 14-16).

As can be seen, the three SLC methods have reached nearly the same command speed from the start-up to 2000 rpm and step-down till their lowest speeds. The CONV method stops at 300 rpm while PP-01 can go down to 200 rpm. The PP-01 method may not work well at speed lower than 200 rpm. This is possibly attributed to the estimated rotor angle being sensitive to the phase lag and magnitude variation of the estimated stator flux linkage. As can be seen, PP-02 can achieve the lowest speed stably at 100 rpm.

The experiments are conducted on the testbench shown in Fig. 13 to compare the operating conditions between CONV and PP-02, as presented in Figs. 17-19.

As can be seen, the estimated load angle with CONV has an increasing error with decreasing speed. In contrast,
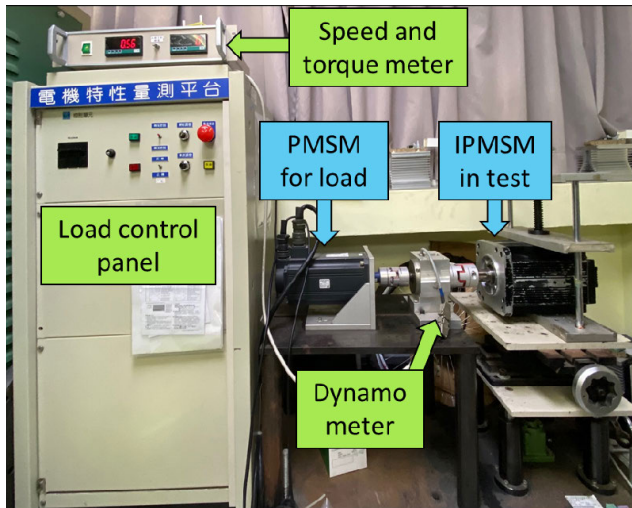
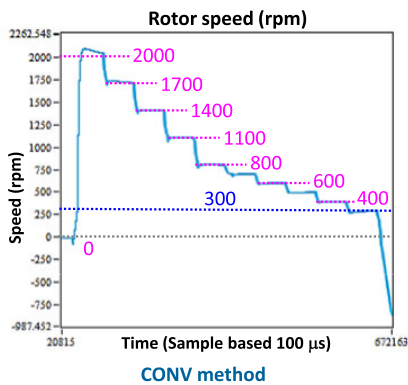FIGURE 13. Experimental setup.

CONV method

FIGURE 14. HIL result of speed response with conventional method (CONV). The horizontal axis is data number with a sampling period of 100 micro seconds. (load: 1Nm).
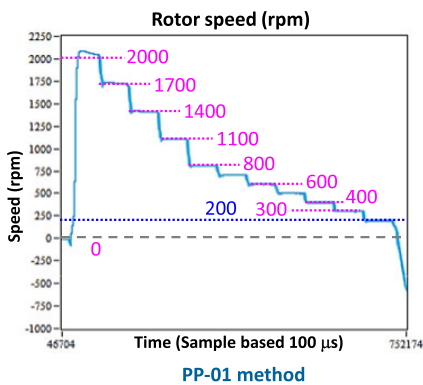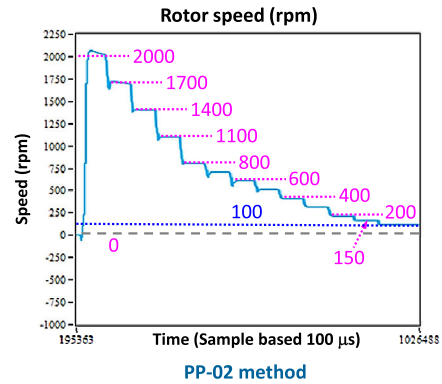

PP-01 method

FIGURE 15. HIL result of speed response with proposed method PP-01. The horizontal axis is data number with a sampling period of 100 micro seconds. (load: 1Nm).

the accuracy of the estimated load angle for the proposed method PP-02 is constantly precise in various conditions. Likewise, the rotor angle accuracy is also significantly enhanced compared to CONV.

C. EFFECTIVENESS OF FINAL PROPOSED METHOD
The SLC FOC drive scheme constructed with PP-02 shown in Fig. 10 is then tested using the testbench in various operating conditions, and the result is shown in Fig. 20. It can be seen

PP-02 method

FIGURE 16. HIL result of speed response with proposed method PP-02. The horizontal axis is data number with a sampling period of 100 micro seconds. (load: 1Nm).
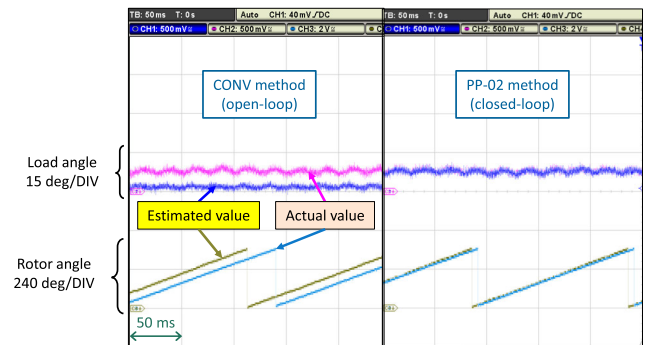

FIGURE 17. The comparison of the load/rotor angle estimation at 100 rpm under load condition 3 Nm (experiment).
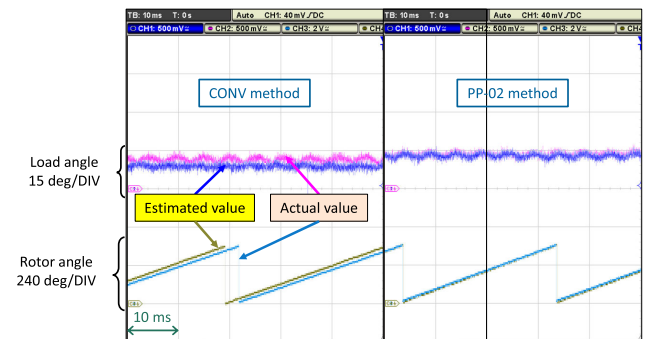

FIGURE 18. The comparison of the load/rotor angle estimation at 500 rpm under full load condition 5 Nm (experiment).
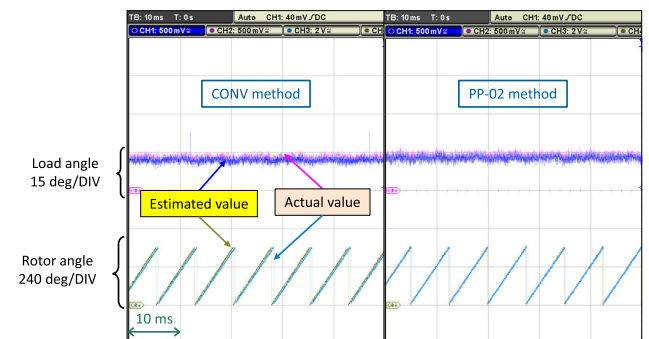

FIGURE 19. The comparison of the load/rotor angle estimation at base speed 2000 rpm under full load condition 5 Nm (experiment).

that the system can operate stably at a wide range, from low to base speed, under various load conditions. However, notable oscillations occur in the rotor angle estimation at 100 rpm,
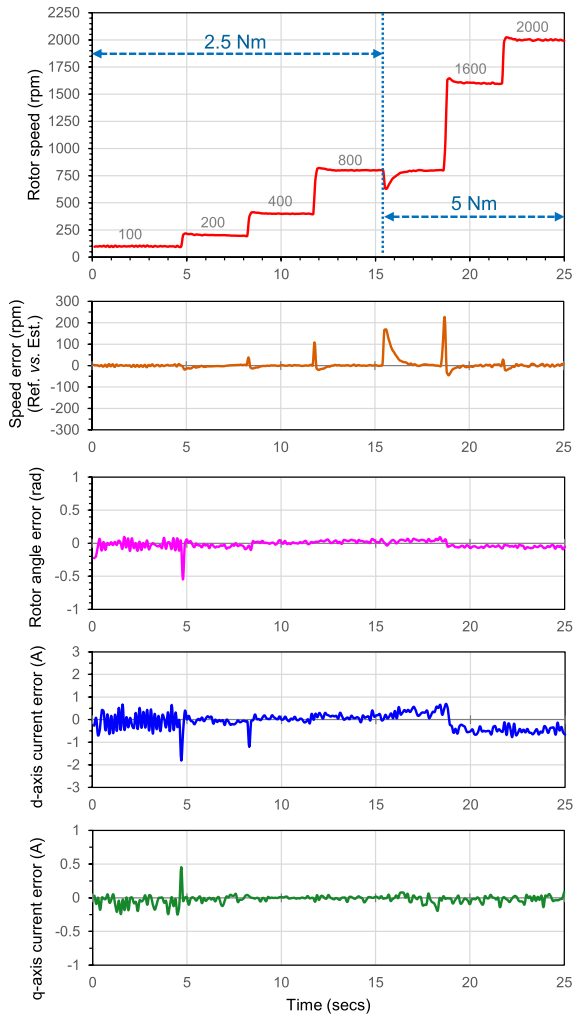
FIGURE 20. Experimental result of PP-02.

FIGURE 21. HIL result at 100 rpm (load 2 Nm) for comparison between (a) normal condition and (b) R_s increase by 30%.

leading to large error and fluctuation in the feedback *d-q*-axis current. This makes the system unable to withstand heavy load or sudden load change at this speed. It should be noted that the B-EMF is small at low speed, and the waveform can be easily affected by large current (causing high voltage drop or saturation) and nonlinearities (e.g., deadtime). From the test results (at 100 rpm) shown in Figs. 17 (3 Nm), 20 (2.5 Nm), and 21 (2 Nm), the error of rotor angle and *d-q*-axis current increase as the load increases. The system becomes stable as beyond 200 rpm. Nevertheless, the LPF estimator used here may not fully eliminate the effect of the nonlinearity on stator flux linkage estimation even at high-speed region. Therefore, the slight error of rotor angle is unavoidable, as shown in Fig. 20. This then results in a slight deviation of feedback *d-q*-axis current through Park transformation with the estimated rotor angle. However, this error seems insignificant since mostly lower than 1 A at the steady state in high speed and heavy load conditions. Hence, the drive system can still perform well.

Furthermore, to check the reliability and robustness of the proposed SLC system, some measurements and evaluations are performed with motor parameter changes, as shown
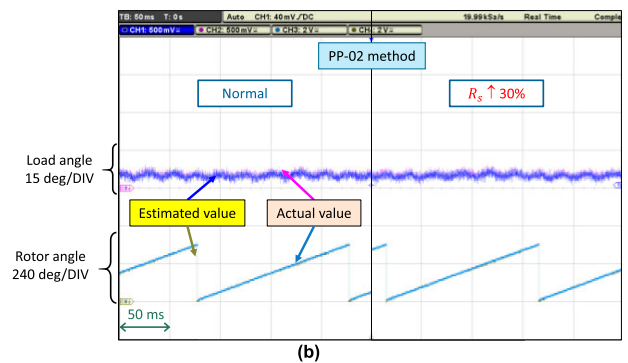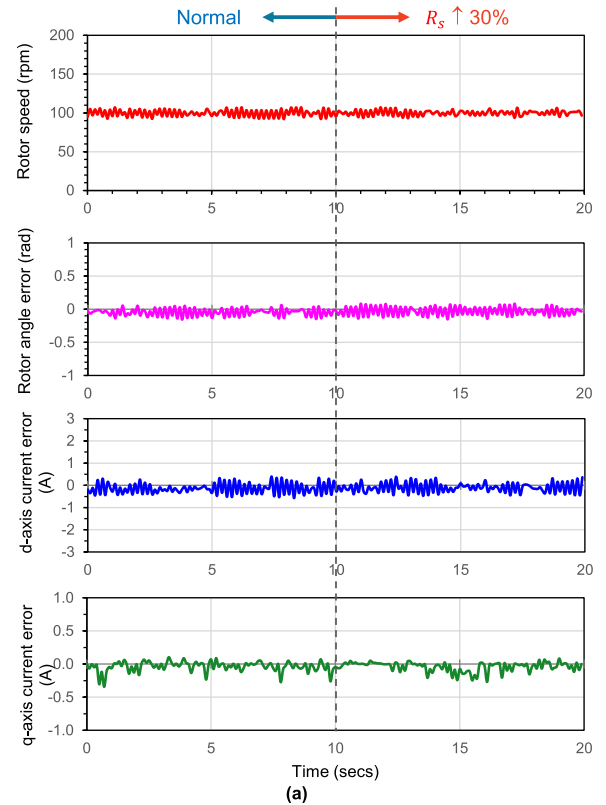
in Figs. 21-24. To vary the motor parameters intentionally, the tests are performed using the HIL. As shown in Fig. 21, if the stator resistance increased by 30%, the system still works normally without any change, even at low speed. However, the speed cannot go further down as the B-EMF could reach a filterable signal-to-noise ratio boundary due to nonlinearity [26] (e.g., deadtime effect).

In the case of a decrease of stator inductances L_d and L_q by 30%, as the results shown in Fig. 22(a), the load angle only drops slightly due to L_q decrease. Note that the variation of L_q is deduced by (36) and updated into the SLC calculation, and consequently, the estimation of rotor position remains accurate with L_q varying, as shown in Fig. 22(b). On the other hand, the effectiveness of the proposed detection approach for PM flux linkage change at high speed is also examined.
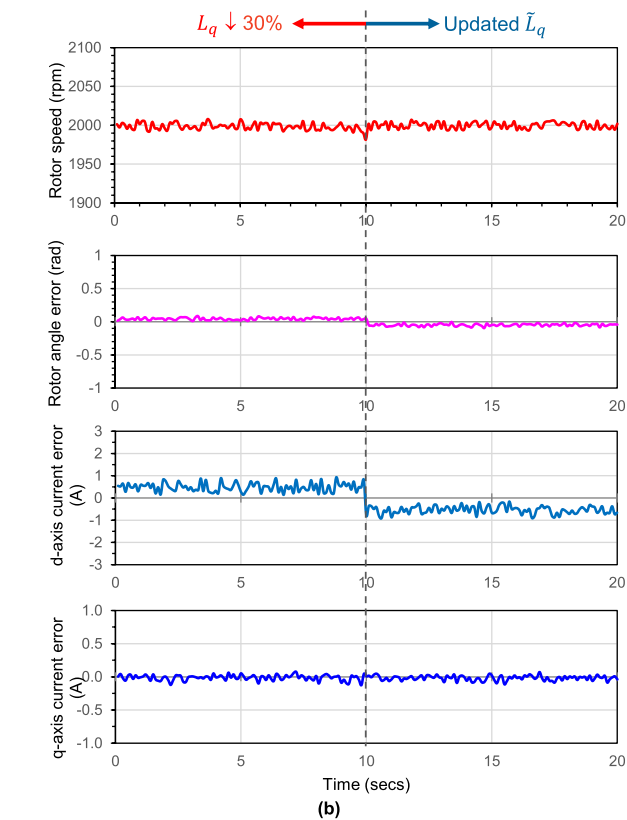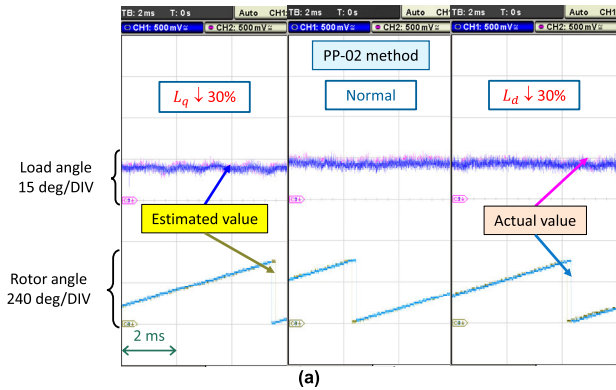
(a)

(b)

FIGURE 22. HIL result at 2000 rpm (load 5 Nm) for (a) comparison between the cases of 30% L_d and L_q reduction and normal condition; (b) before and after updating L_q.
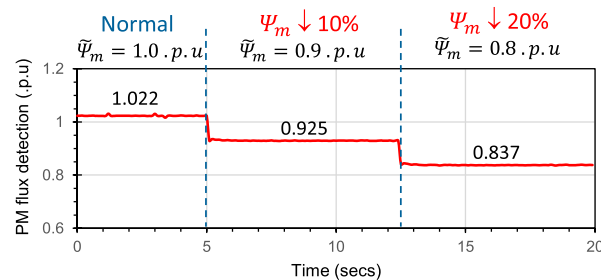

FIGURE 23. HIL result of PM flux linkage variation detected by the proposed method at base speed (2000 rpm).

The detection results are shown in Fig. 23 where the case of 10% PM flux linkage drop has a 0.56% error, and the case of 20% drop has a 2.4% error. This validates the accuracy of
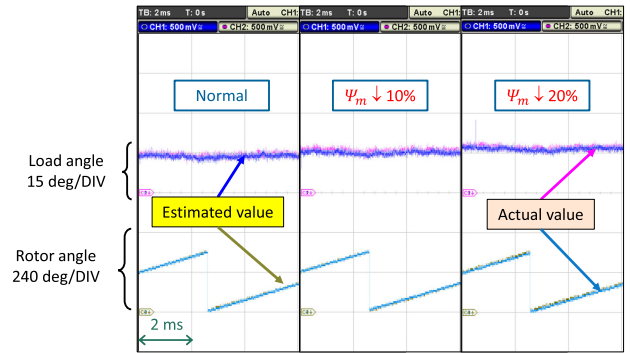

FIGURE 24. HIL result of rotor and load angle estimation after PM flux linkage variation updated by the proposed method at speed 2000 rpm under load 5 Nm.

the proposed detection method. Therefore, the drive system can work stably after the deviation is considered, as shown in Fig. 24, where the reduction of both estimated load angle and rotor position is minor and close to the actual value.

VII. CONCLUSION

In this paper, a novel sensorless technique applied to the PMSM FOC drive based on stator flux linkage has been presented and evaluated. The achievement of this paper can be summed up as:

1) The *d-q*-axis currents can be estimated based on the magnitude of the current and stator flux linkage vector for calculating rotor/load angle for PMSM. It has been demonstrated that this technique can mitigate the effect of stator flux linkage quality on the accuracy of load angle estimation. Thus, the precision and robustness of the rotor angle calculation can be enhanced with the proposed SLC FOC drive.

2) With the phase lag compensation added to stator flux linkage angle at low speed range, the effectiveness of the proposed SLC method has been further enhanced. This allows the PMSM to operate stably at 100 rpm under load condition.

3) The sensitivity to motor parameter variations can be significantly reduced by the proposed sensorless scheme combined with a detection technique.

4) In the proposed SLC scheme, no complicated and extra regulators or filters are needed.

5) The technique using *d-q*-axis current estimation for rotor position calculation and the PM flux linkage detection method proposed in this paper for SLC FOC drives have not been reported elsewhere.

For the limitations of the proposed method, although a robust performance at low speed was demonstrated in this study, other methods are needed to start up the motors.

REFERENCES

[1] A. Mishra, P. Agarwal, and S. Srivastava, "A comprehensive analysis and implementation of vector control of permanent magnet synchronous motor," *Int. J. Power Energy Convers.*, vol. 5, no. 1, pp. 1–23, May 2014.

[2] Q. Wang, S. Wang, and C. Chen, "Review of sensorless control techniques for PMSM drives," *IEEJ Trans. Electr. Electron. Eng.*, vol. 14, no. 10, pp. 1543–1552, Jul. 2019.

[3] G. Wang, M. Valla, and J. Solsona, "Position sensorless permanent magnet synchronous machine drives—A review," *IEEE Trans. Ind. Electron.*, vol. 67, no. 7, pp. 5830–5842, Jul. 2020.

[4] G. De Donato, G. Scelba, M. Pulvirenti, G. Scarcella, and F. G. Capponi, "Low-cost, high-resolution, fault-robust position and speed estimation for PMSM drives operating in safety-critical systems," *IEEE Trans. Power Electron.*, vol. 34, no. 1, pp. 550–564, Jan. 2019.

[5] D. Liang, J. Li, and R. Qu, "Sensorless control of permanent magnet synchronous machine based on second-order sliding-mode observer with online resistance estimation," *IEEE Trans. Ind. Appl.*, vol. 53, no. 4, pp. 3672–3682, Jul./Aug. 2017.

[6] O. C. Kivanc and S. B. Ozturk, "Sensorless PMSM drive based on stator feedforward voltage estimation improved with MRAS multiparameter estimation," *IEEE/ASME Trans. Mechatronics*, vol. 23, no. 3, pp. 1326–1337, Jun. 2018.

[7] S. Bolognani, L. Tubiana, and M. Zigliotto, "Extended Kalman filter tuning in sensorless PMSM drives," *IEEE Trans. Ind. Appl.*, vol. 39, no. 6, pp. 1741–1747, Nov. 2003.

[8] C. M. Verrelli, S. Bifaretti, E. Carfagna, A. Lidozzi, L. Solero, F. Crescimbini, and M. Di Benedetto, "Speed sensor fault tolerant PMSM machines: From position-sensorless to sensorless control," *IEEE Trans. Ind. Appl.*, vol. 55, no. 4, pp. 3946–3954, Jul./Aug. 2019.

[9] D. Xiao, S. Nalakath, S. R. Filho, G. Fang, A. Dong, Y. Sun, J. Wiseman, and A. Emadi, "Universal full-speed sensorless control scheme for interior permanent magnet synchronous motors," *IEEE Trans. Power Electron.*, vol. 36, no. 4, pp. 4723–4737, Apr. 2021.

[10] G. Foo, S. Sayeef, and M. F. Rahman, "Low-speed and standstill operation of a sensorless direct torque and flux controlled IPM synchronous motor drive," *IEEE Trans. Energy Convers.*, vol. 25, no. 1, pp. 25–33, Mar. 2010.

[11] M. F. Rahman, L. Zhong, M. E. Haque, and M. Rahman, "A direct torque-controlled interior permanent-magnet synchronous motor drive without a speed sensor," *IEEE Trans. Energy Convers.*, vol. 18, no. 1, pp. 17–22, Mar. 2003.

[12] M. C. Paicu, I. Boldea, G.-D. Andreescu, and F. Blaabjerg, "Very low speed performance of active flux based sensorless control: Interior permanent magnet synchronous motor vector control versus direct torque and flux control," *IET Electr. Power Appl.*, vol. 3, no. 6, pp. 551–561, Nov. 2009.

[13] I. Boldea, M. C. Paicu, G. D. Andreescu, and F. Blaabjerg, "'Active flux' DTFC-SVM sensorless control of IPMSM," *IEEE Trans. Energy Convers.*, vol. 24, no. 2, pp. 314–322, Jun. 2009.

[14] X. Lin, W. Huang, W. Jiang, Y. Zhao, and S. Zhu, "A stator flux observer with phase self-tuning for direct torque control of permanent magnet synchronous motor," *IEEE Trans. Power Electron.*, vol. 35, no. 6, pp. 6140–6152, Jun. 2020.

[15] G. H. B. Foo and M. F. Rahman, "Direct torque control of an IPM-synchronous motor drive at very low speed using a sliding-mode stator flux observer," *IEEE Trans. Power Electron.*, vol. 25, no. 4, pp. 933–942, Apr. 2010.

[16] C. J. V. Filho, D. Xiao, R. P. Vieira, and A. Emadi, "Observers for high-speed sensorless PMSM drives: Design methods, tuning challenges and future trends," *IEEE Access*, vol. 9, pp. 56397–56415, Apr. 2021.

[17] A. Yousefi-Talouki, P. Pescetto, G. Pellegrino, and I. Boldea, "Combined active flux and high-frequency injection methods for sensorless direct-flux vector control of synchronous reluctance machines," *IEEE Trans. Power Electron.*, vol. 33, no. 3, pp. 2447–2457, Mar. 2018.

[18] C. Wu, X. Sun, and J. Wang, "A rotor flux observer of permanent magnet synchronous motors with adaptive flux compensation," *IEEE Trans. Energy Convers.*, vol. 34, no. 4, pp. 2106–2117, Dec. 2019.

[19] A. K. Jain and V. T. Ranganathan, "Modeling and field oriented control of salient pole wound field synchronous machine in stator flux coordinates," *IEEE Trans. Ind. Electron.*, vol. 58, no. 3, pp. 960–970, Mar. 2011.

[20] J. Hu and B. Wu, "New integration algorithms for estimating motor flux over a wide speed range," *IEEE Trans. Power Electron.*, vol. 13, no. 5, pp. 969–977, Sep. 1998.

[21] W. Xu, S. Qu, L. Zhao, and H. Zhang, "An improved adaptive sliding mode observer for middle- and high-speed rotor tracking," *IEEE Trans. Power Electron.*, vol. 36, no. 1, pp. 1043–1053, Jan. 2021.

[22] Z. Wang, K. Lu, and F. Blaabjerg, "A simple startup strategy based on current regulation for back-EMF-based sensorless control of PMSM," *IEEE Trans. Power Electron.*, vol. 27, no. 8, pp. 3817–3825, Aug. 2012.

[23] M. F. Hsieh, N. C. Chen, and T. T. Ton, "System response of permanent magnet synchronous motor drive based on SiC power transistor," in *Proc. IEEE 4th IFEEC*, Singapore, Nov. 2019, pp. 1–6.

[24] S. Morimoto, M. Sanada, and Y. Takeda, "Wide-speed operation of interior permanent magnet synchronous motors with high-performance current regulator," *IEEE Trans. Ind. Appl.*, vol. 30, no. 4, pp. 920–926, Jul./Aug. 1994.

[25] N. R. N. Idris and A. H. M. Yatim, "An improved stator flux estimation in steady-state operation for direct torque control of induction machines," *IEEE Trans. Ind. Appl.*, vol. 38, no. 1, pp. 110–116, Jan./Feb. 2002.

[26] G.-R. Chen, J.-Y. Chen, and S.-C. Yang, "Implementation issues of flux linkage estimation on permanent magnet machine position sensorless drive at low speed," *IEEE Access*, vol. 7, pp. 164641–164649, Nov. 2019.

[27] L.-J. Cheng and M.-C. Tsai, "Enhanced model predictive direct torque control applied to IPM motor with online parameter adaptation," *IEEE Access*, vol. 8, pp. 42185–42199, Feb. 2020.

[28] M.-F. Hsieh and Y.-C. Weng, "A low torque ripple direct torque control method for interior permanent magnet motor," *Appl. Sci.*, vol. 10, no. 5, p. 1723, Mar. 2020.

THAT-DONG TON (Member, IEEE) was born in Hue, Vietnam. He received the B.S. degree in electrical engineering from the Da Nang University of Science and Technology, Da Nang, Vietnam, in 2006, and the M.S. degree in automation from the Thai Nguyen University of Technology, Thai Nguyen, Vietnam, in 2011. He is currently pursuing the Ph.D. degree in electrical engineering with National Cheng Kung University, Tainan, Taiwan.

His main research interests include power converters and motor drive systems.

MIN-FU HSIEH (Senior Member, IEEE) was born in Tainan, Taiwan. He received the B.Eng. degree in mechanical engineering from National Cheng Kung University (NCKU), Tainan, in 1991, and the M.Sc. and Ph.D. degrees in mechanical engineering from the University of Liverpool, Liverpool, U.K., in 1996 and 2000, respectively.

From 2000 to 2003, he worked as a Researcher with the Electric Motor Technology Research Center, NCKU. He joined the Department of Systems and Naval Mechatronic Engineering, NCKU, as an Assistant Professor, in 2003. He was promoted to a Full Professor, in 2012, and then he joined the Department of Electrical Engineering, in 2017. His research interests include electric machine design, drives, and mechatronics.

Dr. Hsieh was a Senior Member of the IEEE Industry Applications Society, IEEE Magnetics Society, and IEEE Industrial Electronics Society. He has been also an Editor with IEEE TRANSACTIONS ON MAGNETICS and an Associate Editor with IEEE TRANSACTIONS ON INDUSTRY APPLICATIONS.

PO-HSUN CHEN (Member, IEEE) received the Ph.D. degree from the Department of Physics, National Sun Yat-sen University, Kaohsiung, Taiwan, in 2018.

He is currently an Assistant Professor with the Department of Applied Science, R.O.C. Naval Academy, Kaohsiung. His current research interests include developments of nonvolatile memory and various novel electron devices.

• • •